Desalination and Water Treatment
www.deswater.com

doi: 10.5004/dwt.2018.22148

119 (2018) 1–8
July

Physical modifications for improving inlet flow distribution evenness in multiple parallel-arrayed membrane modules

Jiyeong Park[a], Sukmin Yoon[a], Seung-Joon Kim[b], No-Suk Park[a,*]

[a]*Department of Civil Engineering and Engineering Research Institute, Gyeongsang National University, 501, Jinju-daero, Jinju, 52828, Korea, Tel. 82 55 772 1798; Fax: 82 55 772 1799; email: nspark@gnu.ac.kr (N.-S. Park)*
[b]*KOLON GLOBAL Corp., Songdo IT Center, 32, Songdogwahak-ro, Yeonsu-gu, Incheon, Korea*

Received 19 December 2017; Accepted 20 January 2018

ABSTRACT

This study was conducted to validate a proposed hydraulic modification for improving the evenness of the inlet flow distribution in a manifold pipe in a water treatment system in which the treated water flows in parallelly arranged membrane modules, by performing computational fluid dynamics (CFD) simulations and experiments. The results of the CFD simulations confirmed that the coefficient of variation of the flow rate distribution in the manifold pipe could be reduced by approximately 47% by installing an inner orifice pipe within the header pipe (double header pipe). In addition, the experimental results showed that the coefficient of variation was reduced by 67% for a double header pipe compared with a single header pipe. Furthermore, when the diameter of the inner orifice pipe was identical to that of the branch pipe connected to the external header pipe, the flow distribution evenness was maximized.

Keywords: Inlet flow distribution evenness; Computational fluid dynamics; Parallel arranged membrane modules; Double header pipe; Single header pipe

1. Introduction

Application of membrane technology in drinking water treatment offers various advantages such as reduction in the required site area. Numerous microfiltration and ultrafiltration membranes that can be operated at a relatively low pressure have been installed in treatment plants worldwide [1]. A typical low-pressure membrane treatment system configuration is shown in Fig. 1.

Considering this multiple parallelly arranged membrane system simplistically, the inlet water flows from the inlet header pipe, located at the bottom, into each membrane, and the treated water is collected through the outlet header pipe located at the top. A problem with this structure is the unevenness of the flow rate into each module owing to the difference of energy from point to point in pipe. Some researchers in the field of thermodynamic cooling systems have suggested approaches to increase the evenness of the flow rate distribution in a multi-branch pipe (manifold pipe). They recommended that a low ratio of the cross-sectional area of the multi-branch pipe to that of the header pipe could lead to a more even flow distribution [2–4]. Eguchi et al. [5] showed that the head loss decreased as the ratio of the cross-sectional area of the multi-branch pipe to that of the header pipe decreased. However, because the diameter of the inlet pipe for the membrane module is typically set to ~50 mm, there is a limitation in reducing the cross-sectional area of the multi-branch pipe for applying the above methods in a water treatment membrane system. In addition, if the cross-sectional area is reduced, the head loss and energy consumption are increased. Hong and Riggs [6] proposed that a tapered header with a smaller cross-sectional area could achieve a more uniform flow distribution.

In the second half of the 2000s, there were research studies on the design optimization of multi-branch pipes via computational fluid dynamics (CFD). Ding [7] investigated the non-uniform flow rate from the header pipe to the membrane

* Corresponding author.

Presented at the 10th International Desalination Workshop (IDW 2017), November 22–25, 2017, Busan, Korea.

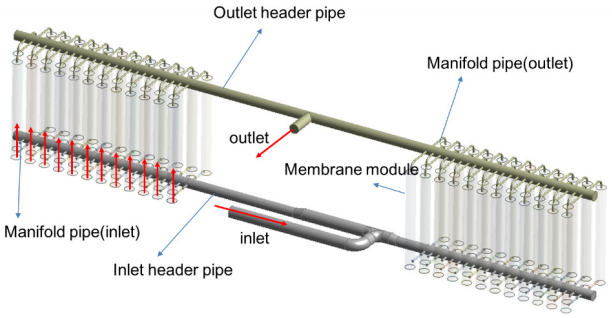

Fig. 1. Typical low-pressure membrane system configuration.

modules that were arranged parallelly, by performing CFD and verification experiments. And he proposed that the addition of new inlet point in the middle of the system could work better from both performance homogeneity and energy consumption point of view. Paul et al. [8] simulated a proton exchange membrane fuel cell stack using CFD and revealed that the fluid flow rate entering the fuel cells arranged in parallel was related to the flow direction of the outflow header. Peng et al. [9] have used CFD to optimize the interconnect channel between thin metal separators in proton exchange membrane fuel cells. Maharudrayya et al. [10] have applied the CFD technique to validate the use of various inlet and outlet shapes to equalize the flow rate of the fluid flowing into the cells arranged in parallel in a proton exchange membrane fuel cell. Seo and Chang [11] have attempted to equalize the flow rates of ammonia injection tubes arranged parallelly in a selective catalytic reduction system using CFD. Poursaeidi and Arablu [12] evaluated various pipe shapes to equalize the steam flow from a combustion tank to a multi-branch pipe using CFD. They suggested four various types of parallel-channel configuration, and proved H-type header has more uniform flow distribution than the other types.

Muhana and Novog [13] examined the effect of the flow rate in the header pipe and Reynolds number on the flow rate distribution in the multi-branch pipe. They revealed that as the Reynolds number increases, the flow rate from the branch pipe far from the header pipe inlet is maximized [13]. As mentioned above, various studies on the distribution of the header and multi-branch pipes have been conducted since the late 2000s. However, most of them are in the field of fuel cells and energy engineering, and there is nearly no research on membrane module piping in the water treatment field.

In this study, to propose a method to improve the inlet flow distribution evenness to multiple parallel-arrayed membranes through a manifold pipe system based on the double piping theory, CFD simulations and verification experiments were performed.

2. Theoretical background

2.1. Double piping theory

Fig. 2 shows simplified single and double manifold header pipes and their energy lines occurring in the case of a relatively low Reynolds number (laminar flow). In this case, the inlet water flows through the header pipe whose head loss increases because of the friction from the side wall. Therefore, the outlet flow rate decreases as the distance of the branch from the inlet increases (Fig. 2(a)). The head loss at the end (right side) is higher than that near the inlet (left side). Fig. 2(b) depicts that inserting an inner orifice pipe within the original single header pipe causes the inlet water to turn at the end of the right side. The friction would cause the head loss at the left side to be higher than at the right side as the inlet water flows from left to right. The head gradient reverses after the main flow turns at the end of the right side, and flows right to left. The head loss and energy level at each branch pipe can be kept constant because the water passes through the orifices in the inner pipe. A comparison of Figs. 2(a) and (b) reveals that the average velocity of a single manifold header pipe can be higher than that of a double manifold header pipe because of the cross-sectional area decrease [14]. This double piping theory is applied to improve the evenness of the flow rate to each branch pipe by inserting an inner orifice pipe into the header pipe.

2.2. Coefficient of variation

To quantitatively evaluate the evenness of the flow distribution into each branch pipe, the coefficient of variation (CV), as shown in Eq. (1), which is a statistical concept, was introduced. The CV is also referred to as the relative standard deviation. It is a measure for comparing the relative dispersions in data groups whose means have different scales. A large CV corresponds to a large relative difference. Im and Son [15] used the CV to estimate the water quality and pollutant loads, such as biochemical oxygen demand, total phosphorous, and total organic carbon. Kwon [16] used the CV as an index to determine the water quality characteristics and identity in the vicinity of a bay. The CV is expressed by the following equation:

$$\mathrm{CV} = \frac{\sigma}{\bar{x}} \tag{1}$$

where σ is the standard deviation and $\bar{x}$ is the arithmetic mean.

3. Materials and methods

3.1. Wet experiments

Fig. 3 shows the actual manifold pipe system used for wet experiments. The system consists of a header pipe, circulating water storage tank, circulation pump, 10 branch pipes, and flow meters. When the circulation pump is operated, the water contained in the circulating water storage tank flows into the header pipe (right side) and is distributed into the 10 branch pipes. The flow introduced into the multi-branch pipe is circulated back to the water storage tank. The inlet flow is introduced from the right side, and the flow rate can be controlled manually. Polyvinyl chloride pipes are not weldable, and so, the header pipe was built using a T-type connector.

The total length of the header pipe is 4.4 m, and the distance between each branch is 350 mm. The inner diameters of the header and inner pipes are 96.2 and 58.2 mm, respectively. The diameter of the inner orifice pipe is 48.6 mm, and each orifice size is 10 mm. The outlet port of the header pipe and orifice position of the inner pipe are identical (Fig. 4).

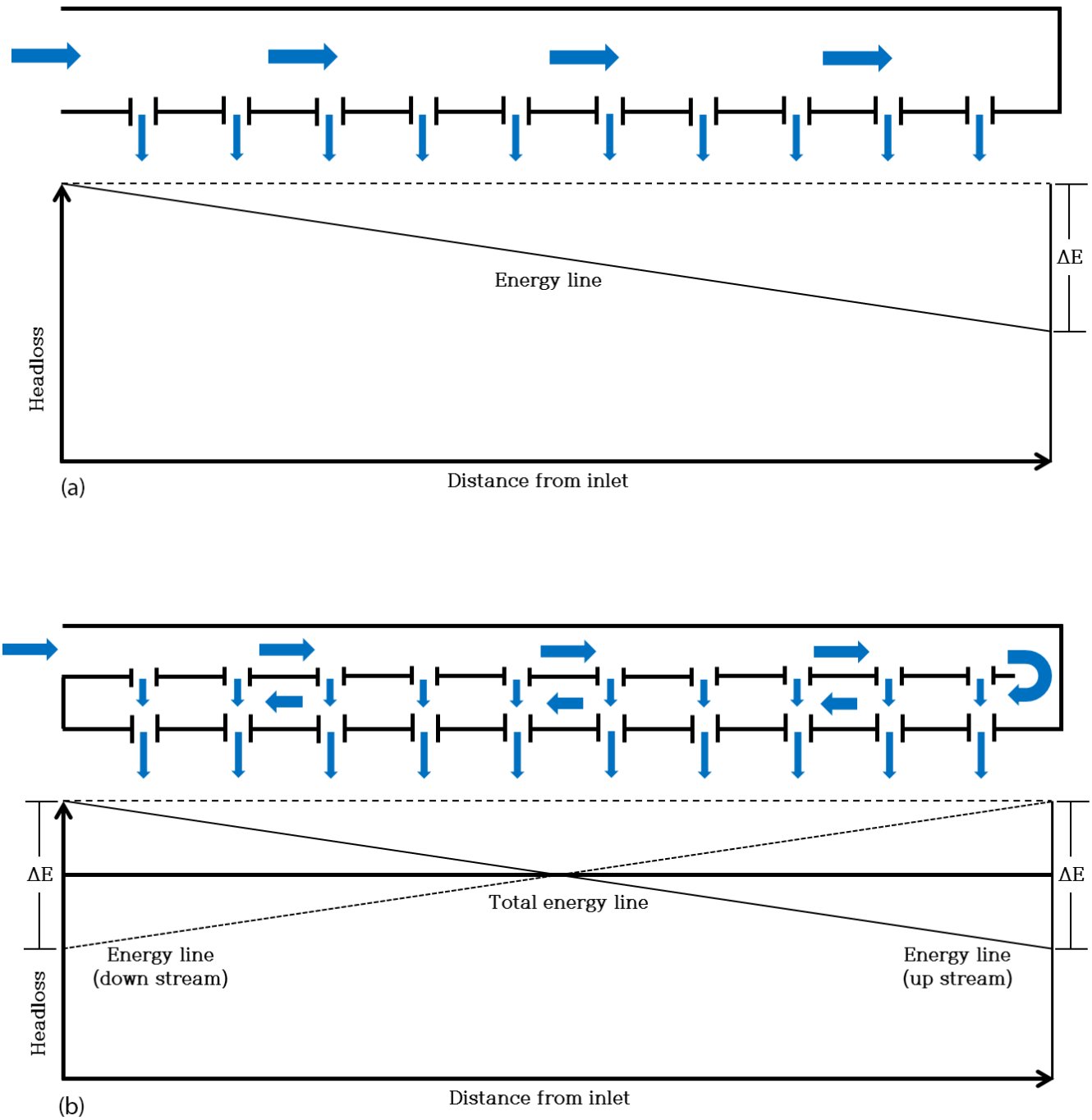

Fig. 2. (a) Single manifold pipe and (b) double manifold pipe and their energy lines.

As shown in Fig. 4, a large plate is placed at the inlet of the inner pipe to prevent water from flowing into the header pipe. The inlet flow rate into the header pipe is 20 m^3/h.

3.2. Methodology of CFD simulations

In this study, the commercial CFD software, ANSYS CFX 16.0 was used to evaluate the evenness of the water distribution within two types of header pipes (single and double header pipes) [17]. The CFD simulation is performed by splitting the geometry of interest into numerous elements, collectively known as grids or cells. Then, the momentum and continuity equations are formulated for each grid together with the given boundary conditions, and they are repeatedly solved by using the finite volume method [18]. A total of 258,809 nodes and 724,387 tetra-shaped cells in the case of the single header pipe, and a total of 597,721 nodes and 1,579,093 cells in the case of the double header pipe were generated, respectively.

Considering that the orifice size of the inner pipe would affect the water flow distribution evenness, the diameter of the orifice was varied by 10% (ratio of the diameter of the orifice to that of the inner pipe) (5 mm), 20% (10 mm), 30% (15 mm), 40% (20 mm), and 50% (25 mm). The CFD simulations were conducted on the assumption of a steady state, and the treated fluid was assumed to be 25°C water, considering the room temperature condition.

The direction of the inner pipe orifice is upward, and the position of the orifice is the same as each branch pipe of the header pipe (refer to Fig. 5).

The time-averaged Navier–Stokes equations for momentum and continuity were solved in this study for achieving a steady, incompressible, turbulent and isothermal flow. The continuity and momentum equations are, respectively,

$$\underline{\nabla}\cdot\left(\underline{U}\right)=0 \tag{2}$$

$$\underline{\nabla}\cdot\left(\rho\underline{U}\otimes\underline{U}-\mu\underline{\nabla U}\right)=\underline{B}+\underline{\nabla}P-\underline{\nabla}\cdot\left(\overline{\rho\underline{u}\otimes\underline{u}}\right) \tag{3}$$

where r and m are the fluid density and dynamic viscosity, respectively. *P* is the pressure, U is the fluid mean velocity, B is the body force, and u is the fluctuating velocity.

The authors assumed that the turbulence in the pipes is isotropic. Therefore, a standard k–ε model was used for modeling the turbulence transport of the momentum. At the pipe wall surface, a no-slip condition was assumed, and a widely used standard wall boundary method was applied to bridge the viscous sublayer. Therefore, it is assumed that the velocity of the component at each wall is zero. The wall shear stress was obtained from the logarithmic law of the wall [18].

4. Results and discussion

4.1. Results of wet experiments

Fig. 6 displays the wet experimental results for the single and double manifold pipes. Water flows into the multi-branch pipe from the right side, and the outlets of the branch pipes are numbered from 1 to 10 from the side closer to the inlet (on the right side).

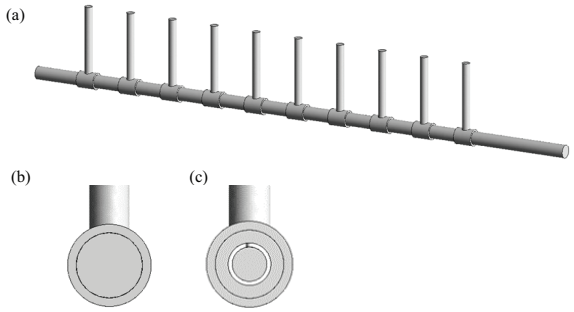

Fig. 5. Geometries of the single and double manifold pipes. (a) Single manifold pipe (3D view), (b) single manifold pipe (front view) and (c) double manifold pipe (front view).

Fig. 3. Manifold pipe system for wet experiments.

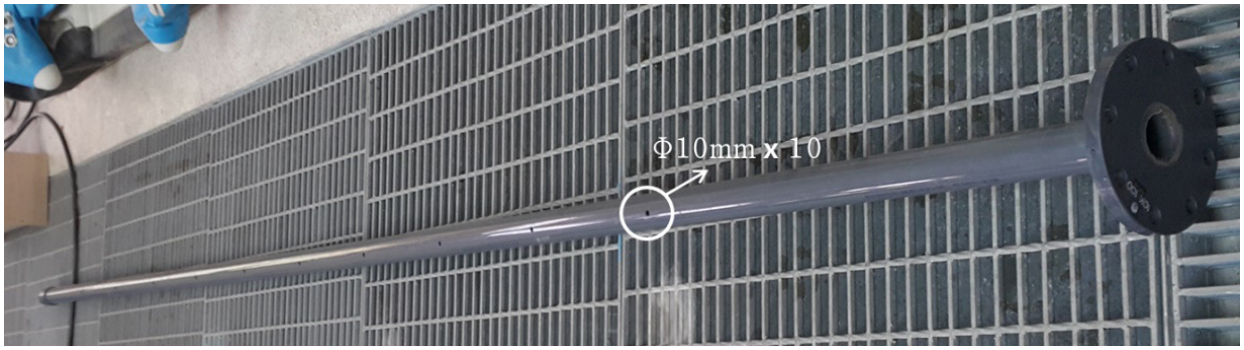

Fig. 4. Inner orifice pipe for the double header pipe.

As shown in Fig. 7, it can be confirmed that for the double manifold pipe applying the double piping theory, the outflow is relatively more even. In the experiment, the outflow rate of 'out1' was measured to be relatively higher than the other outflow rates in the case of a single header pipe. The difference in the outflow flow rate was relatively small for the double header pipe. In addition, as explained in Fig. 2(a), single manifold pipe, the outflows near the inlet are higher. And those far from the inlet tend to decrease. Conversely, inserting an inner orifice pipe within the header pipe reduces the cross-sectional area and accelerates the flow velocity in header pipe, allowing the inlet energy to be transferred to the end of the pipe.

Table 1 summarizes the flow rate distributions and CVs of the different outlet ports. With the single header pipe, the flow rate of 'out1' is the highest at 5.400 m^3/h, whereas the flow rate of 'out10' is the lowest at 1.080 m^3/h. The difference between the maximum and minimum flow rates is 4.320 m^3/h. In the case of the double header pipe based on the double piping theory, 'out6' and 'out10' flow rates are the highest at 2.400 m^3/h, whereas 'out1' flow rate is the least at 1.200 m^3/h, and the difference between them is 1.200 m^3/h. Calculating the CVs for both the cases, values of 0.707 and 0.230 are obtained for the single and double header pipes, respectively. This confirms that the double header pipe flow case is approximately 67% more than the single header pipe flow.

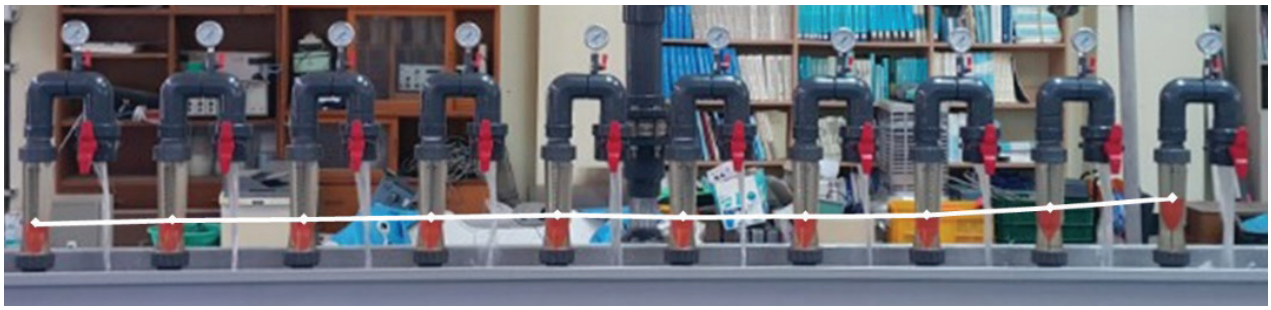

(a)

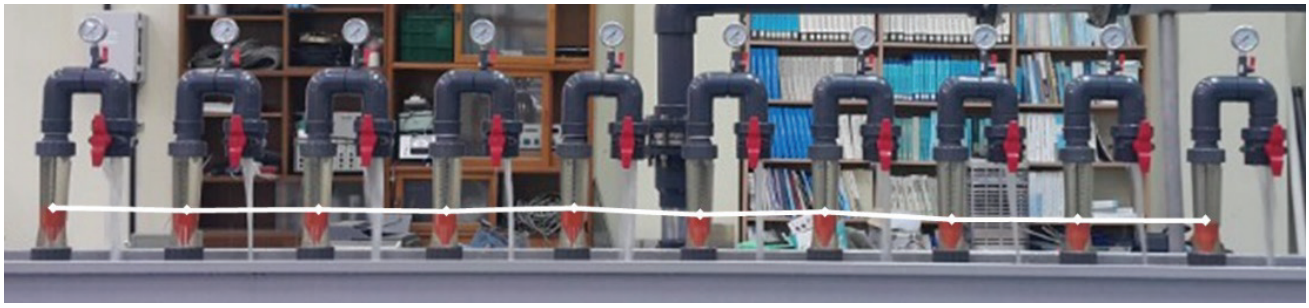

(b)

Fig. 6. Results of the wet experiments (photos). Experimental result for (a) the single manifold pipe and (b) the double manifold pipe.

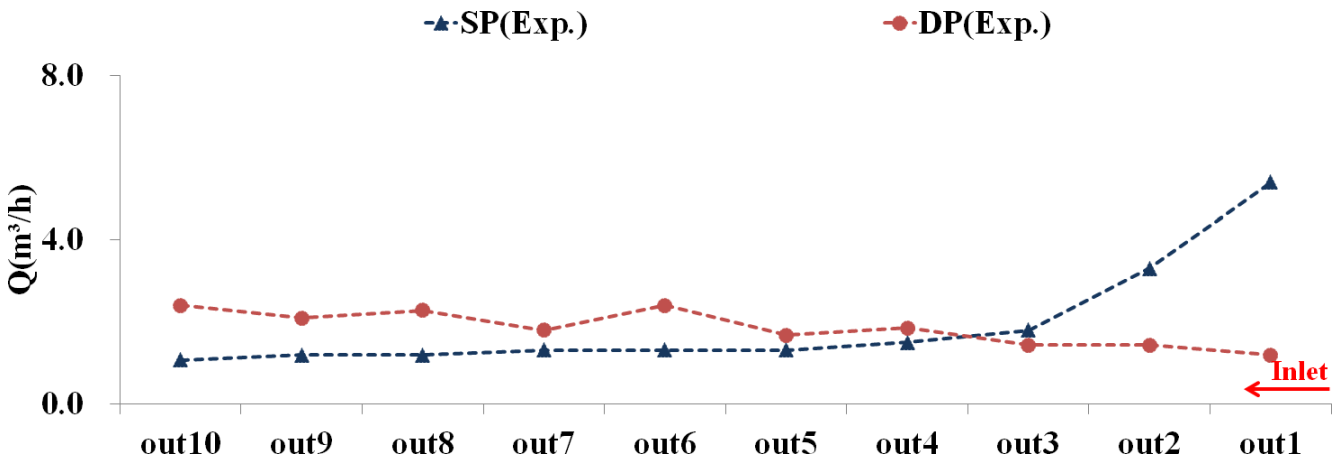

Fig. 7. Results of the wet experiments (SP: single header pipe, DP: double header pipe).

4.2. Results of CFD simulations

Fig. 8 shows the CFD simulation results as a graphical representation for various double header pipe geometries. 'DP(CFD)_5mm' represents the case where the diameter of the orifice in the inner pipe within the double header pipe is 5 mm, which is approximately 10% of the inner pipe diameter. It is shown that a larger orifice diameter of the inner pipe indicates more flow will be distributed to the end (the left side).

Fig. 9 displays the CVs of the above five cases. In case of DP(CFD)_10mm, the CV is 0.154 that is significantly lower than that of the other cases. As can be seen from the simulation results, the orifice diameter of the inner pipe has a significant effect on the flow distribution. And it can be recognized that the orifice diameter should not exceed 20% of the inner pipe diameter. When the orifice diameter exceeds 20%, it can be seen that the larger the diameter, the lower the evenness of the flow rate. These simulated results were reflected in the wet experiments for designing the inner orifice pipe size.

The CFD simulation results are represented as contours, as shown in Fig. 10. The legend range indicates that the blue part is 0 m/s and red part is at least over 2 m/s. In the case of a single manifold pipe (Fig. 10(a)), the main horizontal velocity drops sharply owing to the resistance from the wall friction from the surface irregularities. The velocity within the left half of the header pipe is depicted in blue. In contrast, in the case of the double header pipe under the double piping theory, the red color represents the fast flow rate that appears up to 'out6'. In addition, the flow rate is distributed more evenly in each outlet.

Table 1
Flow rate distributions and CVs from the wet experiments

	out10	out9	out8	out7	out6	out5	out4	out3	out2	out1	CV
Single (m^3/h)	1.080	1.200	1.200	1.320	1.320	1.320	1.500	1.800	3.300	5.400	0.707
Double (m^3/h)	2.400	2.100	2.280	1.800	2.400	1.680	1.860	1.440	1.400	1.200	0.230

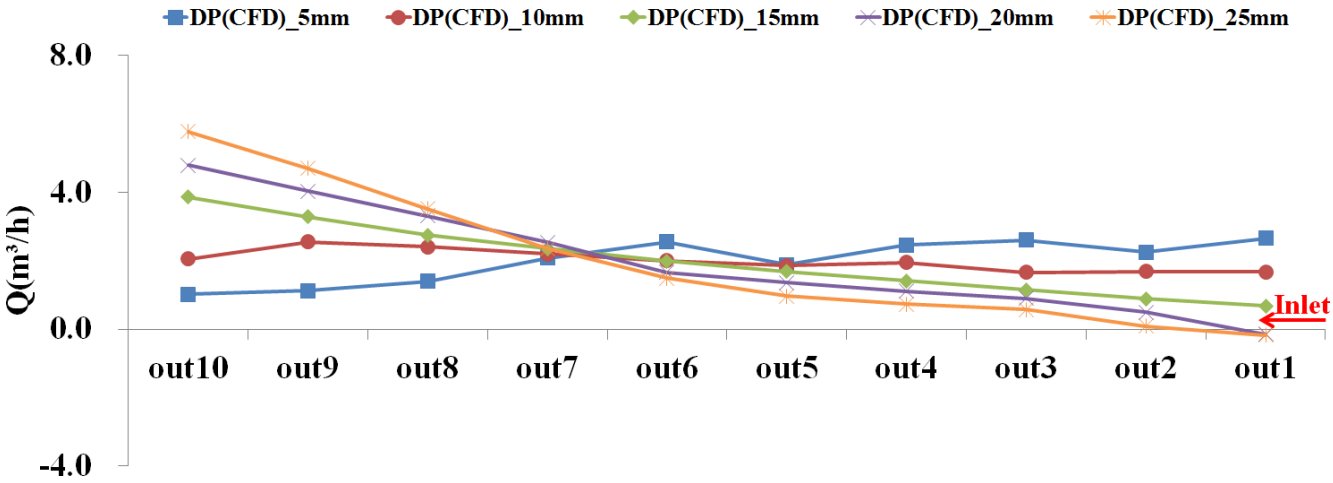

Fig. 8. Results of the CFD simulations (DP_#: double header pipe_orifice diameter mm).

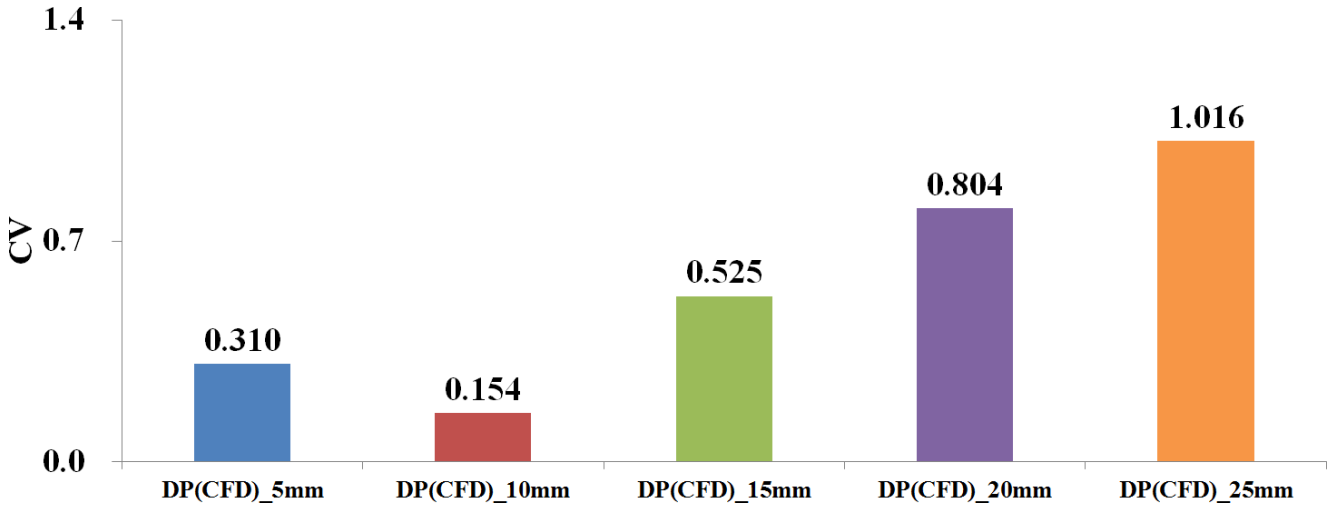

Fig. 9. CVs from the CFD simulations (DP_#: double header pipe_orifice diameter mm).

Fig. 11 is a graphical representation of the CFD simulation results for the single and double manifold pipes. This graph shows the flow rate flowing out through each branch pipe. In the case of a single manifold pipe, the flow rates out of the front half part (out1–5) are relatively higher than those of the rear part (out6–10). In contrast, in the case of the double manifold pipe, the flow rate of the rear part is slightly higher. Comparing both the pipes, the maximum flow rate for the double manifold pipe is much smaller.

Table 2 summarizes the flow rates and CVs for each pipe to quantitatively compare the CFD simulation results. In the case of the single manifold pipe, the flow rate from 'out3' port is the highest at 2.873 m^3/h, whereas the flow rate of 'out9' is the lowest at 1.404 m^3/h, and the difference between the maximum and minimum flow is found to be 1.469 m^3/h. In the case of the double manifold pipe under the double piping theory, the flow rate from 'out9' is the highest at 2.551 m^3/h, whereas the flow rate of 'out3' is the lowest at 1.688 m^3/h, and the difference between the maximum and minimum flow rates was found to be 0.863 m^3/h. In addition, the CVs were derived to be 0.292 and 0.154 for the single and double header pipes, respectively. Consequently, the double header pipe flow rate is approximately 47% more even than the single header pipe flow rate.

It can be seen that there is a difference between the flow rates and CVs obtained from both the CFD simulations and wet experimental results. In the case of the CFD simulation, the entire pipe wall was assumed to be completely smooth, but the actual roughness of the pipe could not be known. The difference between the CFD simulations and wet experimental

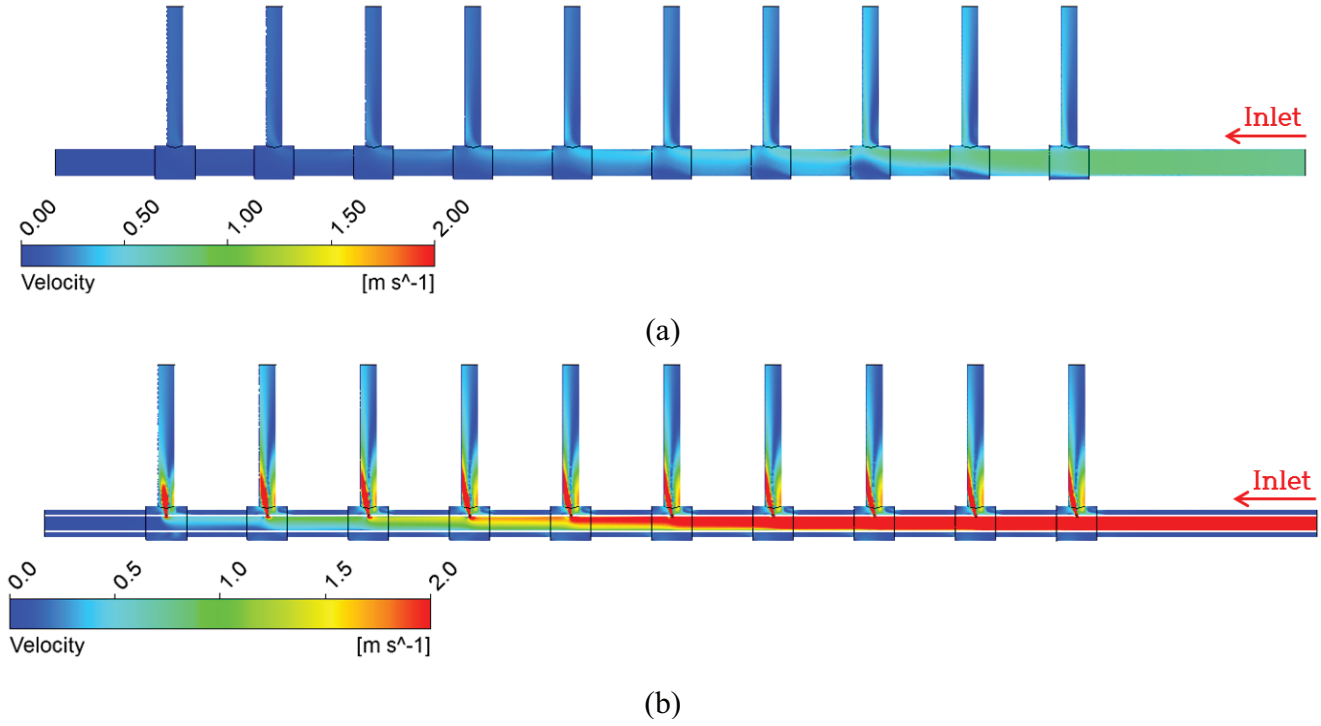

Fig. 10. Results of the CFD simulations. Velocity contour of (a) single manifold pipe and (b) double manifold pipe.

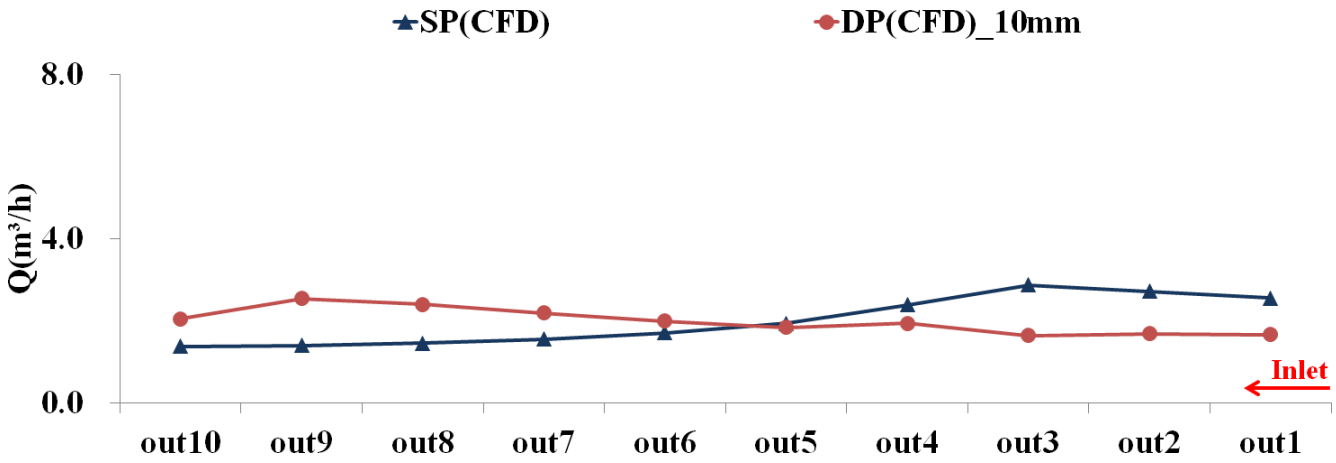

Fig. 11. Comparison of single and double manifold pipes (CFD simulations).

Table 2
Flow rate distribution and CVs from the CFD simulations

	out10	out9	out8	out7	out6	out5	out4	out3	out2	out1	CV
Single (m^3/h)	1.379	1.404	1.457	1.561	1.713	1.943	2.390	2.873	2.723	2.559	0.292
Double (m^3/h)	2.054	2.551	2.400	2.196	1.996	1.848	1.946	1.651	1.688	1.672	0.154

results is owing to the lack of the roughness coefficient of the pipes constituting the experimental apparatus. In conclusion, the CFD simulations and experimental results showed that the flow distribution within the double manifold pipe is considerably more even than within the single manifold pipe.

5. Conclusion

Conducting CFD simulations and verification experiments, the authors suggested a method to improve the inlet flow distribution evenness to multiple parallel-arrayed membranes through a manifold pipe system based on the double piping theory. Through this study, the following conclusions were drawn:.

- The method proposed in this study, that is, applying the double piping theory to the manifold pipe, was confirmed to improve the inlet flow distribution evenness to multiple parallel arrayed membranes through a manifold pipe system.
- From the results of the CFD simulation, it was confirmed that the CV of the flow rate distribution from the manifold pipe could be reduced by ~47% by inserting an inner orifice pipe within the header pipe (double header pipe). In addition, the experimental results showed that the CV was reduced by 67% for the double header pipe compared with the single header pipe.
- In addition, the orifice diameter of the inner pipe has a significant effect on the flow distribution. The orifice diameter should not exceed 20% of the inner pipe diameter for even flow distribution. When the orifice diameter exceeds 20%, it can be seen that the larger the diameter, the lower the evenness of the flow rate.

Acknowledgment

This work was supported by the International Cooperation Program for Technologies (N0001232) funded by the Korea government Ministry of Trade, Industry and Energy.

References

[1] H. Yamamura, K. Kimura, Y. Watanabe, Mechanism involved in the evolution of physically irreversible fouling in microfiltration and ultrafiltration membrane used for drinking water treatment, Environ. Sci. Technol., 41 (2007) 6789–6794.
[2] P.I. Shen, The effects of friction on the flow distribution in diving and combing flow manifold, J Fluids Eng., 114 (1992) 121–124.
[3] S.H. Choi, S. Shin, Y.I. Cho, The effect of area ratio on the flow distribution in liquid cooling module manifolds for electronic packaging, Int. Commun. Heat Mass Transfer, 20 (1993) 221–234.
[4] A.B. Datta, A.K. Majumdar, Flow distribution in parallel and reverse flow manifolds, Int. J. Heat Mass Transfer, 2 (1990) 253–262.
[5] A. Eguchi, M. Kuragasaki, Y. Sueoka, Performance Improvement on ACDEFLO Headbox of Paper Machine, Mitsubishi Heavy Industries Technical Review, Vol. 25, 1988, pp. 191–196.
[6] J.C. Hong, J.B. Riggs, Flow distribution in tapered, rectangular cross section manifolds, J. Chin. Inst. Chem. Eng., 18 (1987) 193–202.
[7] W. Ding, Application of CFD in Membrane Technique, Doctor Dissertation, Universität Duisburg-Essen, 2012.
[8] A.C.C. Paul, S. Jean, S. Jürgen, W. Brian, Flow distribution in proton exchange membrane fuel cell stacks, J. Power Sources, 162 (2006) 340–355.
[9] H. Peng, P. Linfa, Z. Weigang, L. Xinmin, Optimization design of slotted-interdigitated channel for stamped thin metal bipolar plate in proton exchange membrane fuel cell, J. Power Sources, 187 (2009) 407–414.
[10] S. Maharudrayya, S. Jayanti, A.P. Deshpande, Pressure drop and flow distribution in multiple parallel-channel configurations used in proton-exchange membrane fuel cell stacks, J. Power Sources, 157 (2006) 358–367.
[11] M. Seo, H. Chang, Computational study on design of the AIG for the enhancement of ammonia injection in the SCR system, Clean Technol., 18 (2012) 410–418.
[12] E. Poursaeidi, M. Arablu, Using CFD to study combustion and steam flow distribution effects on reheater tubes operation, J. Fluids Eng., 133 (2011) 1–11.
[13] A. Muhana, D.R. Novog, Validation of Fluent for Prediction of Flow Distribution and Pressure Gradients in a Multi-branch Header under Low Flow Conditions, Proc. 16th International Conference on Nuclear Engineering, ICONE16, May 11–15, Orlando, Florida, USA, 2008.
[14] J. Park, S. Kim, Y. Jeong, S. Yoon, N. Park, Effects of inlet flow distribution evenness on outlet water quality from multiple parallel-arrayed sedimentation basins, Desal. Wat. Treat., 61 (2017) 120–125.
[15] T.H. Im, Y.G. Son, Water quality analysis in Nakdong River tributaries, J. Environ. Sci. Int., 25 (2016) 1661–1671.
[16] J.N. Kwon, Characteristic of long term variation of the water quality at the waters of Goseong bay, J. Korean Soc. Mar. Environ. Energy., 13 (2010) 279–287.
[17] ANSYS Corp, Ansys CFX-Solver Modeling Guide Release 15.0, Canonsburg, USA, 2013.
[18] N. Park, S. Kim, Y. Lee, C. Wang, Effects of longitudinal baffles on particles settling in a sedimentation basin, Water Sci. Technol., 69 (2014) 1212–1218.